www.nature.com/cdd

CDDpress

ARTICLE

Check for updates

Transcription factor Zhx2 is a checkpoint that programs macrophage polarization and antitumor response

Siyu Tan[1,2,6], Zehua Wang[2,3,6], Na Li[2], Xiaowei Guo[2], Yankun Zhang[2], Hongxin Ma[2,4], Xueqi Peng[2], Ying Zhao[2], Chunyang Li[5], Lifen Gao[2], Tao Li[1], Xiaohong Liang[2]✉ and Chunhong Ma[2]✉

Macrophages are usually educated to tumor-associated macrophages (TAMs) in cancer with pro-tumor functions by tumor microenvironment (TME) and TAM reprogramming has been proposed as a potential tumor immunotherapy strategy. We recently demonstrated the critical role of Zinc-fingers and homeoboxes 2 (Zhx2) in macrophages' metabolic programming. However, whether Zhx2 is responsible for macrophage polarization and TAMs reprogramming is largely unknown. Here, we show that Zhx2 controls macrophage polarization under the inflammatory stimulus and TME. Myeloid-specific deletion of *Zhx2* suppresses LPS-induced proinflammatory polarization but promotes IL-4 and TME-induced anti-inflammatory and pro-tumoral phenotypes in murine liver tumor models. Factors in TME, especially lactate, markedly decrease the expression of Zhx2 in TAMs, leading to the switch of TAMs to pro-tumor phenotype and consequent cancer progression. Notably, reduced ZHX2 expression in TAM correlates with poor survival of HCC patients. Mechanistic studies reveal that Zhx2 associates with NF-κB p65 and binds to the *Irf1* promoter, leading to transcriptional activation of *Irf1* in macrophages. Zhx2 functions in maintaining macrophage polarization by regulating *Irf1* transcription, which may be a potential target for macrophage-based cancer immunotherapy.

Cell Death & Differentiation (2023) 30:2104–2119; https://doi.org/10.1038/s41418-023-01202-4

INTRODUCTION

Primary liver cancer, which predominantly consists of hepatocellular carcinoma (HCC), ranks as the fifth most common primary cancer and the third most common cancer-associated cause of death [1]. Despite advances in both identifying risk factors and therapeutic options, the incidence of liver cancer is increasing, and patients' survival remains unsatisfactory [2]. Liver cancer usually develops from a background of the persistent presence of inflammation which is accompanied by infiltration with enormous immune cells [3, 4]. Among them, macrophages, termed tumor-associated macrophages (TAMs) are the most abundant immune subsets which play critical roles in orchestrating the immunosuppressive microenvironment. A growing body of evidence demonstrates the positive correlation of increased density of TAMs with early recurrence and poorer survival in patients with liver cancer [5, 6]. Approaches aiming at TAMs are therefore attractive and promising as immunotherapy strategies [7].

Macrophage is a plastic cell type capable of reacting to microenvironment cues [8]. Lipopolysaccharide (LPS) or IFN-γ activate transcription factors (TFs), such as interferon regulatory factors (IRFs) and nuclear factor kappa B (NF-κB) to mount an inflammatory response with high production of IL-1β, IL-6, and TNF-α [9, 10]. In contrast, macrophages respond to cytokines IL-4 and IL-13, effectively turning on signature anti-inflammatory genes such as arginase (Arg1) and TGF-β. Based on the pro-inflammatory and anti-inflammatory functions of macrophages under different stimuli, macrophages are classically classified into activated M1 or anti-inflammatory M2. These pro- and anti-inflammatory pathways can converge with one another [11]. Accumulating evidence shows that macrophage polarization is transient, and the plasticity of macrophages depends on environmental stimuli. This is especially important in the context of TAMs. Microenvironmental factors imposed by the tumor microenvironment (TME), including origins of tumors, metabolic contexts, and cytokine milieus, have been suspected to tailor pro-tumorigenic features and mitigate anti-tumorigenic features, making macrophage plasticity [12]. The presence of M1-macrophage is generally associated with a better prognosis in solid tumors [13], whereas high M2-macrophage numbers are associated with increased angiogenesis, metastasis, and a poor prognosis in several cancer types [14, 15]. Considerable efforts have been decided over the past decade at the depletion or neutralization of M2-like TAMs, or repolarization toward M1-like phenotype [16]. However, the impact of TAM-targeting therapies on the immunological profiles of TAMs has not been fully elucidated. Moreover, although plenty of TFs that control M1/M2

[1]Department of General Surgery, Qilu Hospital, Shandong University, Jinan, China. [2]Key Laboratory for Experimental Teratology of Ministry of Education, Key Laboratory of Infection and Immunity of Shandong Province and Department of Immunology, School of Basic Medical Sciences, Qilu Hospital, Cheeloo Medical College of Shandong University, Jinan, Shandong, China. [3]Department of Clinical Laboratory, Qilu Hospital, Shandong University (Qingdao), Qingdao, China. [4]Department of Clinical Laboratory, Shandong Cancer Hospital and Institute, Shandong First Medical University, and Shandong Academy of Medical Sciences, Jinan, China. [5]Key Laboratory for Experimental Teratology of Ministry of Education, Department of Histology and Embryology, School of Basic Medical Sciences, Cheeloo Medical College of Shandong University, Jinan, Shandong, China. [6]These authors contributed equally: Siyu Tan, Zehua Wang. ✉email: liangxiaohong@sdu.edu.cn; machunhong@sdu.edu.cn

Received: 18 July 2022 Revised: 22 July 2023 Accepted: 2 August 2023
Published online: 15 August 2023

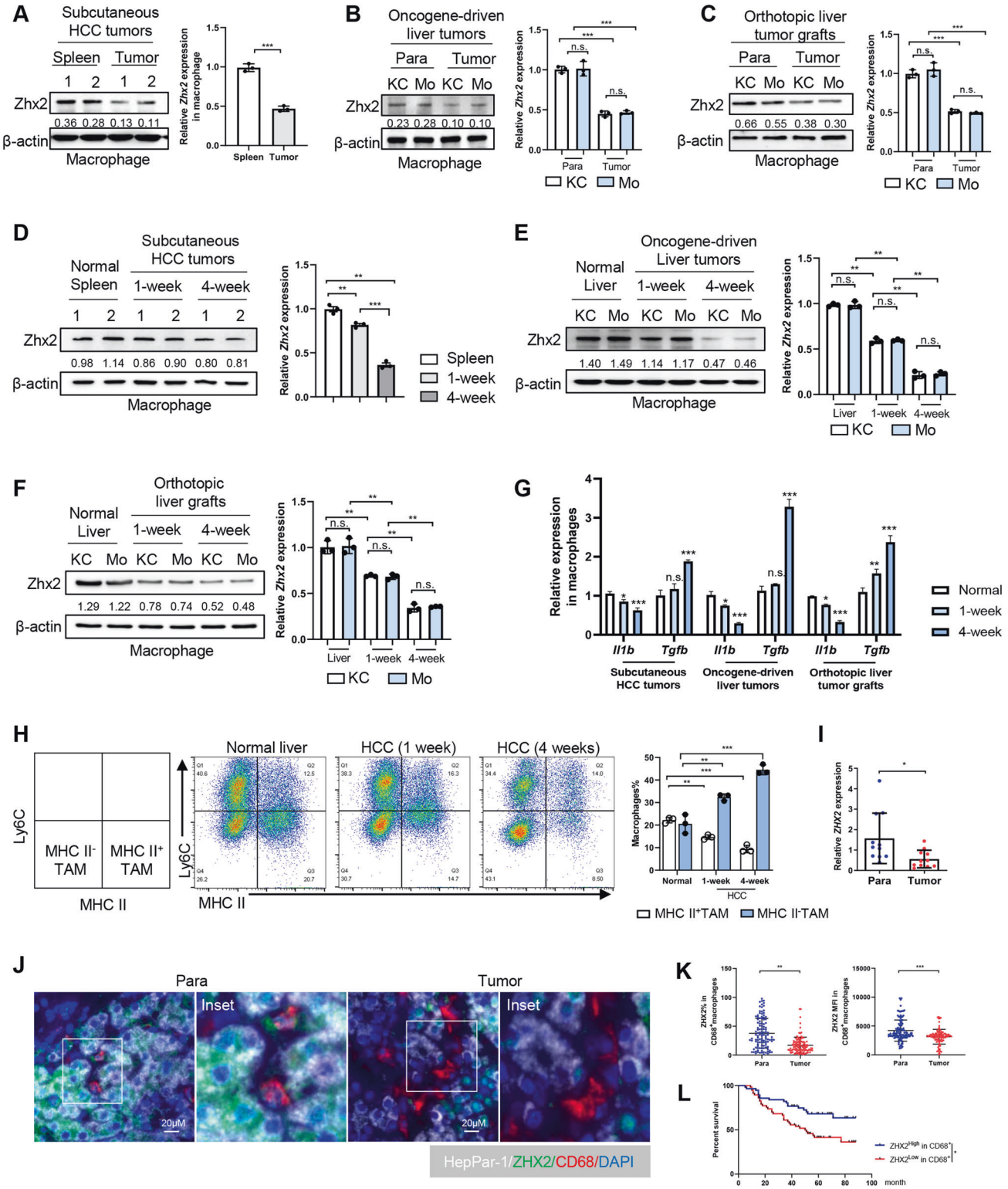

polarization have been identified, it remains uncertain whether TFs for M1/M2- macrophage polarization are also crucial for TAM differentiation.

Zinc-fingers and homeoboxes 2 (Zhx2) is a member of a small gene family that acts as ubiquitous TFs [17]. Accumulated data reveal the important role of Zhx2 in various physiological and pathological processes including neuron development, B cell differentiation, hemopoietic and solid tumor progression [18, 19]. Functioning as a tumor suppressor, Zhx2 inhibits liver cancer progression by transcriptional repression of genes related to cell proliferation, lipid metabolism, and self-renew [20–22]. Northern blot assay demonstrates the abundant expression of Zhx2 in immune organs including the spleen and thymus [17]. We recently identified Zhx2 as the key regulator controlling NK cell maturation [23]. More interestingly, a transcription factor network study of human monocytic THP-1 cells has shown that ZHX2, acting as one

Fig. 1 Reduced expression of Zhx2 in tumor associated macrophages. A Zhx2 expression in macrophage from subcutaneous HCC tumors and spleen from tumor-bearing mice. Macrophages were sorted by FACS Aria. Macrophages: Dead$^-$ CD45$^+$ CD11c$^-$ CD11b$^+$ F4/80$^+$. Western blot (left), actin was used as the loading control, and the relative gray value (Zhx2/β-actin) was calculated by *Image J* software. Realtime QPCR analysis (right). Zhx2 expression in macrophage subsets from the liver of para-tumoral and tumoral tissues of *Akt/cMyc* driven orthotopic liver tumor model (**B**) and orthotopic liver grafts model (**C**). Macrophages were sorted by FACS Aria. Kupffer cell (KC): Dead$^-$ CD45$^+$ CD11c$^-$ CD11b^{low} F4/80^{high}. Monocyte-derived inflammatory macrophage (Mo): Dead$^-$ CD45$^+$ CD11c$^-$ CD11b^{high} F4/80^{low}. Western blot (left), actin was used as the loading control, and the relative gray value (Zhx2/β-actin) was calculated by *Image J* software. Realtime QPCR analysis (right). Zhx2 expression in TAM from the murine subcutaneous liver tumor (**D**), oncogene-driven orthotopic liver tumors (**E**), and orthotopic liver grafts (**F**) at early (1 week) or late (4 weeks) stage. **G** Realtime-QPCR analysis of *Il1b* and *Tgfb* expression in TAM of tumors from (**D**) to (**F**). **H** FCM analysis of macrophage phenotype in oncogene-driven liver tumor in mice at an early or late stage. MHC II$^+$ macrophage: Dead$^-$ CD45$^+$ CD11c$^-$ CD11b$^+$ F4/80$^+$ MHCII$^+$ Ly6C$^-$, MHC II$^-$ macrphage: Dead$^-$ CD45$^+$ CD11c$^-$ CD45$^+$ CD11b$^+$ F4/80$^+$ MHCII$^-$ Ly6C$^-$. **I** Realtime-QPCR analyzed *ZHX2* expression in macrophage from para-tumoral and tumoral tissues of HCC patients. Multiplex immunofluorescence staining of ZHX2, CD68, or HepPar-1 in human liver cancer tissue array. Representative multiplex immune-histochemistry images (**J**), summary plots of ZHX2 percentage and mean fluorescence intensity (MFI) were analyzed in each group (**K**). Each symbol represents data from an individual patient. **L** Overall survival analysis of HCC patients with a high or low percentage of ZHX2$^+$ cells in CD68$^+$ TAMs from tumor regions. HCC tissues were classified into two groups according to ZHX2$^+$ percentage. The cut-off for the grouping was determined by the median expression of ZHX2. Data were analyzed using Student's t-test (two-tailed unpaired *t* test) in (**A**–**I**, **K**), and using log-rank (Mantel-Cox) test in (**L**.) * <0.05, **<0.01, ***<0.001, **** <0.0001, n.s., no significance.

of the critical locks avoiding a transcriptional avalanche, appears to both be highly regulated and be able to participate in the regulation of nearly 300 genes, which indicate that Zhx2 may play an important role in macrophages [24] Consistent with this, recent work demonstrated that Zhx2 promotes macrophage survival in atherosclerotic lesions [25] and that its high expression in LPS-stimulated macrophages is essential for promoting macrophage glycolysis and inflammatory responses during sepsis [26]. However, it is unclear whether Zhx2 is expressed in immunosuppressive TAMs and how Zhx2 regulate macrophage polarization under different stimulus, especially in liver cancer.

In the current study, we demonstrate that Zhx2 is a critical regulator that controls macrophage polarization under both inflammatory and anti-inflammatory stimuli. Especially, lactate in TME reduces the expression of Zhx2 in macrophages which in turn promotes the development of liver cancer through enhancing the polarization of TAM into pro-tumoral phenotype. Mechanically, the Zhx2-NF-κB p65 complex binds to the *Irf1* promoter region in macrophages, leading to transcriptional activation. Our data reveal transcription factor Zhx2 as a checkpoint of macrophage polarization in the tumor microenvironment.

RESULTS

Zhx2 expression is downregulated in TAMs and correlates with poor survival of liver cancer patients

TAMs, as a well-recognized core element of TME, play crucial roles in tumor progression [27, 28]. To explore the potential involvement of Zhx2 in TAMs, we measured Zhx2 expression in TAMs and different macrophage subsets. Flow cytometry confirmed the purity of isolated splenic macrophages (Fig. S1A), hepatic macrophage subsets (Kupffer cells (KC), and monocyte-derived macrophages (Mo)) (Fig. S1B). Although Zhx2 expression did not differ either in KC and Mo from either tumor and para tumor liver tissues (Fig. 1B, C) or in macrophages from spleen and liver (Fig. S1C), Zhx2 expression was reduced in TAMs from subcutaneous HCC tumors (Fig. 1A), oncogene-driven liver tumors (Fig. 1B) and orthotopic liver tumor grafts (Fig. 1C). Moreover, Zhx2 expression was further decreased when tumor progressed into late stage (4 weeks after tumor implantation) (Fig. 1D–F). TAMs are highly dynamic and heterogeneous [29]. Consistently, TAM developed a more anti-inflammatory phenotype in late-stage tumors (Fig. 1G). We found the proportion of MHC II$^+$macrophagese which was reported as a proinflammatory subset [29, 30] continued to decrease, whereas MHC II$^-$ macrophages were accumulated during liver tumor development (Fig. 1H). Intriguingly, Zhx2 expression was significantly higher in MHC II$^+$ TAMs but lower in MHC II$^-$ TAMs (Fig. S1D, E). The decreased ZHX2 in TAMs was further verified in human HCC tissues. As shown in Fig. 1I and Fig. S1F, S1G, real-time qPCR analysis detected significantly lower *ZHX2* in TAMs isolated from human HCC tissues than that in macrophages from the paired surrounding non-cancerous tissues.

The next crucial question is whether Zhx2 expression in TAMs is relevant to human liver cancer progression. To address this, multiplex immunofluorescence staining was used for the detection of CD68 and ZHX2 in the liver cancer tissue array (Figs. 1J, S1H). As shown in Fig. 1K, both percentage of ZHX2$^+$CD68$^+$ macrophages and mean fluorescence intensity (MFI) of ZHX2 staining in CD68$^+$ macrophages were greatly lower in human liver tumors than that in adjacent normal liver (para-tumor) tissue. Notably, ZHX2^{low} in CD68$^+$ macrophage significantly correlated with poor survival of liver cancer patients (Fig. 1L). In accordance, *ZHX2* expression was positively correlated with the infiltration of macrophages in TCGA-LIHC data (TIMER (harvard.edu)) (Fig. S1I). All these demonstrated that Zhx2 expression is selectively downregulated in TAMs in HCC and is correlated with liver cancer progression.

Elevated lactate in TME decreases Zhx2 expression in TAMs

To further explore the factor that reduces Zhx2 expression in TAMs, BMDMs from WT mice were stimulated with HCC conditioned medium (HCM) prepared from the culture supernatant of murine and human liver cancer cell lines as previously reported to mimic TME [31]. As shown in Fig. S2A, HCM from murine liver tumor cells Hepa1-6 greatly decreased Zhx2 expression in BMDMs and the reduction of *Zhx2* showed HCM-dose dependent manner. This was further confirmed with human monocytic THP-1 cells. As shown in Fig. S2B, HCM from human HCC cell line Huh7 cells markedly decreased ZHX2 expression in THP-1 cells in a time-dependent manner. Also, treatment with tissues homogenate from human HCC tissues significantly downregulated ZHX2 expression in THP-1 cells (Fig. S2C, D).

In tumors, macrophages are exposed to a broad range of stimuli which was categorized into two main groups: danger signals, and homeostatic, metabolic signals. To ascertain the potent factor contributing to the decrease of Zhx2 in TME, we size-fractionated the conditioned medium and control medium into two fractions bearing the >3 kDa or <3 kDa molecules. As shown in Fig. 2A, treatment with unfractionated total HCM and the HCM fraction of <3 kDa but not the HCM fraction of >3 kDa significantly reduced *Zhx2* expression in BMDMs, suggesting that factor(s) repressing *Zhx2* expression in HCM are low molecular weight. Moreover, boiled HCM maintained its ability to repress *Zhx2* expression (Fig. 2B), which further suggested the potential role of heat-stable metabolites. To further define the major small molecule

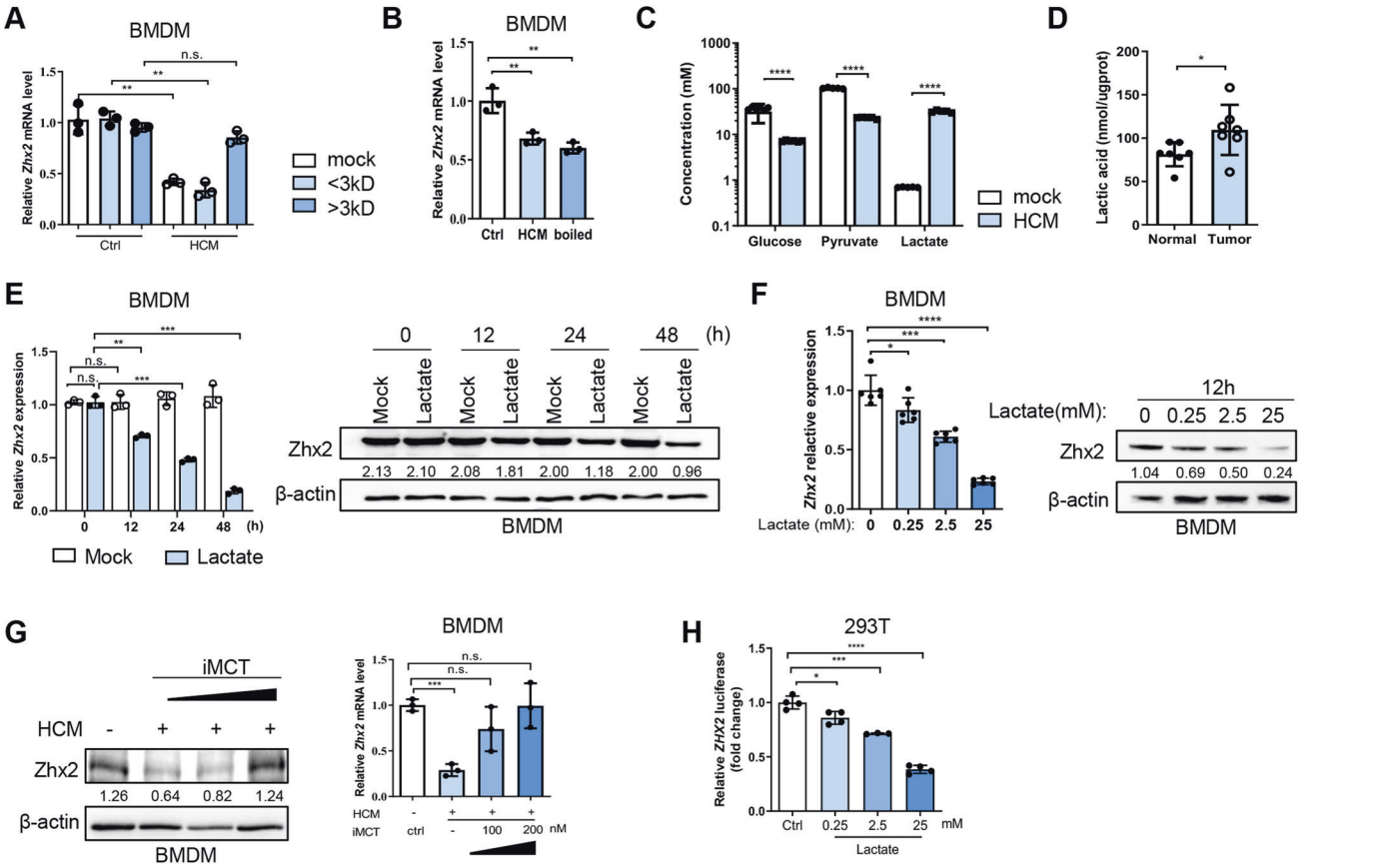

Fig. 2 Lactate suppressed Zhx2 expression in TAM. Realtime-QPCR analysis of *Zhx2* in murine BMDMs stimulated with indicated treatments. Ultrafiltration centrifugation was used to size-fractioned the conditional medium into two fractions bearing the >3 kDa or <3 kDa molecules (**A**). Boiled HCM was heated at 100 °C for 5 min using metal bath heating (**B**). **C** Colorimetry analysis of the concentration of carbohydrate metabolism by-productions (glucose, pyruvate, lactate) in Hepa1-6 derived HCM. **D** Colorimetry determined lactate content in para-tumor liver tissues and tumor tissues from HCC patients. Western blotting (left) and Realtime-QPCR analysis (right) of Zhx2 in BMDMs stimulated with 2.5 mM lactate for the indicated time (**E**) or stimulated 12 h with the indicated concentration of lactate (**F**), or stimulated with HCM with or without 1 μM MCT inhibitor (iMCT) (**G**). **H** Luciferase activity of ZHX2 promoter reporter plasmid (ZHX2-luc) in lactate stimulated 293 T cells. Luciferase activity was measured 48 h post-transfection. Data are represented as mean ± S.D. Each data point represents 1 sample. Data were analyzed using Student's t-test (two-tailed unpaired t-test) in **A**–**H**, * <0.05, **<0.01, ***<0.001, **** <0.0001, n.s. no significance.

contributing to the reduction of Zhx2 in TAMs, we measured common solute factors of <3 kDa in HCM. As expected, lactate, glucose, and pyruvate were detected in Hepa1-6 HCM. In particular, the level of lactate was about 30 folds higher in HCM than control medium (Fig. 2C). The increased lactate was verified in tumor tissue from clinic HCC samples (Fig. 2D). Consistent with a previous report demonstrating lactate as the dominant metabolite promoting TAMs reprograming [32], lactate significantly reduced Zhx2 expression in BMDMs in a time- and dose-dependent manner (Fig. 2E, F). Furthermore, blocking lactate transporter with an increased dose of monocarboxylic acid transport inhibitor (iMCT, MedChemExpress, *Cat#HY-119996A*, New Jersey, U.S.) significantly blocked the HCM-induced reduction of Zhx2 expression in BMDMs (Fig. 2G). In accordance, luciferase reporter assay showed that lactate reduced the *ZHX2* promotor activity in 293T cells in a dose-dependent manner (Fig. 2H). Together, these data illustrate that the increased lactate in TME reduces Zhx2 expression in TAMs.

Depletion of *Zhx2* in macrophages promotes tumor growth both in vitro and in vivo

To investigate the functional relevance of macrophage Zhx2 in tumor growth, BMDMs derived from myeloid-specific *Zhx2* knockout mice (referred to as MKO mice) and $LysM^{cre}$-$Zhx2^{f/f}$ littermate mice (referred to as WT mice) were stimulated with HCM to mimic TAMs, and these TAMs were then co-cultured with murine hepatoma cell line Hepa1-6 cells. Western blotting and Realtime QPCR verified the efficient knockout of *Zhx2* in macrophages and TAMs but not in hepatocytes and T cells (Fig. S3A, B). Results of transwell and CCK-8 assay showed that deletion of *Zhx2* in HCM-stimulated macrophages largely promoted the migration and proliferation of cocultured Hepa1-6 tumor cells (Fig. S4A, B), suggesting that *Zhx2* loss in TAM leads to accelerated tumor cell growth. In accordance, compared with WT BMDMs, both lactate- (Fig. S4C, D) and IL-4- (Fig. S4E, F) stimulated MKO BMDMs displayed an enhanced ability to promote cell proliferation and migration of hepatoma Hepa1-6 cells.

To validate the role of Zhx2 in enhancing the tumor-suppressive ability of macrophages in vivo, subcutaneous Hepa1-6 homografts were separately prepared in MKO and WT mice (Fig. 3A). As shown in Fig. 3B, Hepa1-6 homograft grew much faster and bigger in MKO mice than that in WT mice. The increased expression of Ki67(Fig. S4G) and Pcna (Fig. S4H) confirmed the enhanced proliferation of tumor cells in MKO mice. To further solidify the role of Zhx2 in TAMs in liver cancer, three kinds of hepatoma murine models were prepared in MKO and WT mice, including STZ-HFD induced in situ liver tumors [22, 33] (Fig. 3C), oncogene-driven liver tumors prepared by hydrodynamic injection of

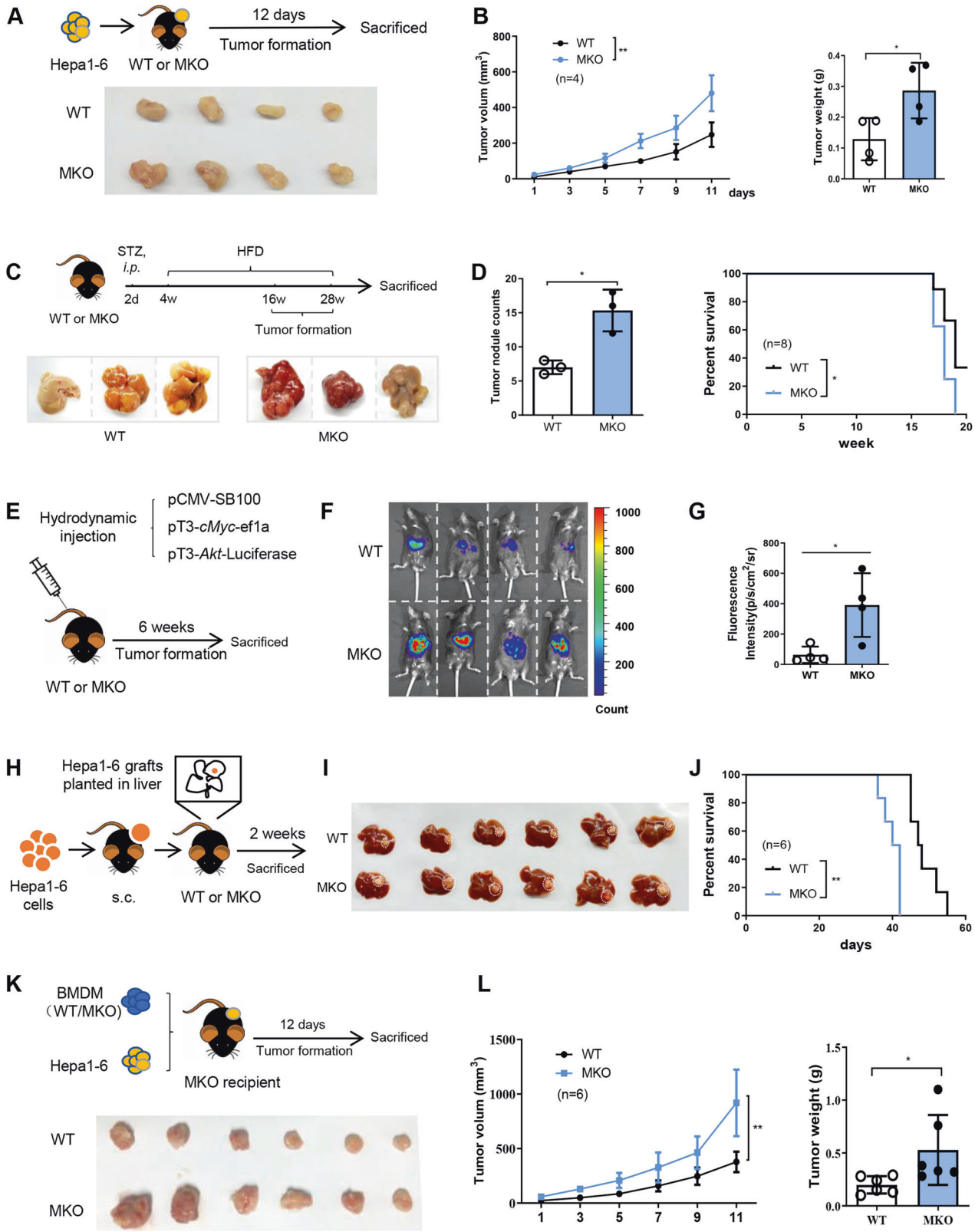

sleeping beauty transposon and *Akt/cMyc*-luc plasmid [34] (Fig. 3E), and orthotopically transplanted Hepa1-6 grafts (Fig. 3H). As shown in Fig. 3D, F, G, and I, loss of *Zhx2* in myeloid cells led to significantly increased tumor growth in all tested murine live tumor models. Notably, MKO mice showed poorer survival than WT mice in both STZ-HFD-induced HCC and orthotopically implantation models of HCC (Fig. 3D, J).

To access whether the promotion of myeloid-specific deletion of *Zhx2* on tumor cell growth was intrinsic to macrophages, BMDMs from MKO or WT mice were mixed with Hepa1-6 cells and

Fig. 3 Deficiency of Zhx2 in macrophages aggravated tumor burden. Tumor growth and weight in WT or MKO mice subcutaneously transplanted with Hepa1–6 cells (1×10^6). Experimental design and tumor image (**A**), tumor growth, and weight (**B**) are shown ($n = 4$ for each group). The liver tumor model was established by feeding 24 weeks of high-fat diet (HFD) after injection of 20 μg streptozotocin (STZ) at 2 days after birth in WT or MKO mice. The experimental design and tumor imaging (**C**), numbers of tumor nodules, and survival curves (**D**) are shown. A liver tumor model was prepared by hydrodynamic tail vein injection of Akt/cMyc plasmids and sleeping beauty transposon SB100 in WT and MKO mice. Experimental design (**E**), tumor burden screened by IVIS Spectrum (**F**), and tumor size displayed by fluorescence screen (**G**) were shown. Experimental scheme (H), tumor image (**I**), and survival curve (**J**) of WT or MKO mice orthotopically transplanted with Hepa1-6 grafts in the liver. Tumor growth and weight in MKO mice subcutaneously transplanted with Hepa1-6 cells (1×10^6) mixed with BMDMs (1×10^6) from WT or MKO mice. Experimental design, tumor image (**K**), tumor growth, and weight (**L**) are shown. Data are represented as mean ± S.D. Each data point represents an individual mouse. Data were analyzed using Student's t-test(two-tailed unpaired t-test) in (**B**) (right), (**D**) (left), (**G**), and (**L**) (right), using a two-way ANOVA test in (**B**) (left), (**L**) (left), and using log-rank (Mantel-Cox) test in (**D**) (right), (**J**). * <0.05, **<0.01.

then subcutaneously injected into MKO mice (Fig. 3K). As expected, co-injection with *Zhx2*-deficient BMDMs led to significantly increased tumor growth and the tumor grafts were larger in the MKO group than those in WT control (Fig. 3K, L), suggesting that Zhx2 in macrophages inhibits tumor progression. To further exclude the role of neutrophils and confirm the role of macrophages, neutrophils were depleted by anti-Ly6G antibody (BioxCell, New Hampshire, USA) in WT or MKO mice, and the growth of the Hepa1-6 subcutaneous tumor was evaluated. As shown in Fig. S5A–D, administration of anti-Ly6G antibody could not abrogate the difference in tumor growth between WT and MKO mice. This confirmed that neutrophil does not contribute to enhanced tumor growth in MKO mice. Taken together, the above data demonstrate that deficiency of *Zhx2* in macrophages effectively promotes liver tumor growth.

Deletion of *Zhx2* switches TAMs to pro-tumor phenotype and shapes the suppressive TME in murine liver cancer

M2 polarization of TAMs is key for tumor progression. To further investigate the role of Zhx2 in TAMs polarization, BMDMs from WT and MKO mice were stimulated with Hepa1-6 HCM or lactate for 24 h, mimicking the promotion of TME-educated TAMs. Realtime-QPCR assay showed that deletion of *Zhx2* increased the expression of M2 markers, such as *Arg1*, *CD206*, and *Tgf-β* in HCM and lactate educated-TAMs (Fig. S6A, B), consistent with our previous study reporting the involvement of Zhx2 in promoting macrophages glycolysis and the well-defined enhanced OXPHOS in M2 macrophages [26].

Tumor progression is associated with the anti-inflammatory function of TAMs, resulting in the exhaustion of CTLs. Accordingly, using the TCGA-LIHC patient bulk RNA-seq datasets, we found the enrichment of T cells exhaustion signature and TAMs signature in the $ZHX2^{low}$ group compared with the $ZHX2^{high}$ group (Fig. S7A). To further verify the Zhx2 mediated pro-tumor TAMs polarization in vivo, infiltrated macrophages were freshly isolated from subcutaneous Hepa1-6 homograft (Fig. 4A), STZ-HFD induced liver tumors (Fig. 4F), and orthotopically transplanted Hepa1-6 grafts (Fig. 4K) from WT and MKO mice. Flow cytometry assay showed that both the number and the percentage of tumor-infiltrated macrophages were less in MKO mice than that in WT mice (Fig. S7B–E). To distinguish macrophages from other myeloid cells in TME, TAMs were gated on $CD45^+dead^-CD11b^+F4/80^+CD11c^-Gr\text{-}1^-Ly6C^-SiglecF^-$subsets and subtyped by MHC II (Fig. S7B). Phenotypically, TAMs isolated from MKO mice showed significantly increased levels of CD206, Arg1, and TGF-β in MHC II^- macrophages, and decreased TNF-α expression in MHC II^+ macrophages, regardless of whether TAMs were isolated from Hepa1-6 homograft (Fig. 4B, C), metabolic induced-liver tumor (Fig. 4G, H) or orthotopic liver homografts (Fig. 4L, M). In addition, to verify the effects of *Zhx2* in regulating polarization of different liver macrophage subsets in TME, oncogene-driven HCC models were induced in WT and MKO mice and KC and monocyte-derived macrophages (Mos) were analyzed (Fig. S8A). As expected, knockout of *Zhx2* leads to an anti-inflammatory phenotype in both $CD11b^+F4/80^{high}Tim\text{-}4^+$ KCs and $CD11b^+F4/80^{low}Tim\text{-}4^-$ Mos, as increased expression of Arg1 (Fig. S8B) and decreased expression of IL-6 (Fig. S8C). Moreover, consistent with the well-recognized role of TAMs in orchestrating immunosuppressive microenvironment, MKO mice have fewer tumor-infiltrating $CD8^+$ T cells (Fig. S7F–H) and higher expression of immune checkpoints PD-1 and Tim-3 in infiltrating $CD8^+$ T cells (Fig. 4D, I and N). Also, the percentage of Treg cells was greatly increased in MKO mice than in WT mice (Fig. 4E, J, and O).

Collectively, these results confirm that loss of *Zhx2* promotes the polarization of TAM to protumor M2 phenotype and enhances the immunosuppressive microenvironment in liver cancer. These observations suggest that the Zhx2-dependent TAM programming generally promotes a suppressive immune microenvironment in malignancies.

Zhx2 expression in macrophages is highly regulated and crucial for macrophages polarization in adaption to both inflammation and TME

Previous studies suggested Zhx2 as a TF which is highly regulated in human THP-1 cells [24]. We then came to describe the expression pattern of Zhx2 in macrophages under different stimuli. As shown in Fig. S9, LPS promoted (Fig. S9A, B) while IL-4 (Fig. S9C, D) repressed *Zhx2* expression in RAW264.7 cells, and the regulation showed a time or dose-dependent manner. Together with the results showing the downregulated Zhx2 expression in TAMs and in macrophages treated with HCM and lactate, our data suggest that Zhx2 expression is highly regulated in macrophages, which is consistent with the previous computational study [24].

LPS and IL-4 are two well-identified stimulators promoting macrophage M1/M2 polarization. We, therefore, hypothesized that Zhx2 might participate in LPS/IL-4-mediated macrophage polarization. To address this, global RNA-sequencing analysis was performed with BMDMs from *PRJNA598552*. The volcano plot from RNA-seq showed that 5727 genes significantly altered in the MKO group compared with the WT group (Fig. S9E). Gene pathway analysis revealed that the cytokine signaling and immune response pathway were significantly overrepresented, further supporting the involvement of Zhx2 in the regulation of macrophages (https://www.kegg.jp/kegg/rest/keggapi.html) (Fig. S9F). To better understand the regulation of Zhx2 on macrophages, we analyzed the pathway enriched in differentially expressed genes (DEGs) between *Zhx2*-deficient macrophages and control macrophages. As shown in Fig. 5A, gene pathway analysis revealed that the negatively regulated immune process was enriched in MKO while the positively regulated immune process was enriched in WT. Moreover, GSEA analysis showed that signatures of immunogenic classical M1 phenotype and transcripts associated with inflammatory response were enriched in BMDMs from WT mice (Fig. 5B). To obtain more in-depth insights into the impact of *Zhx2* loss on the macrophage-related inflammatory response, we compared the representative inflammatory-related genes in WT and MKO BMDMs. Heatmap

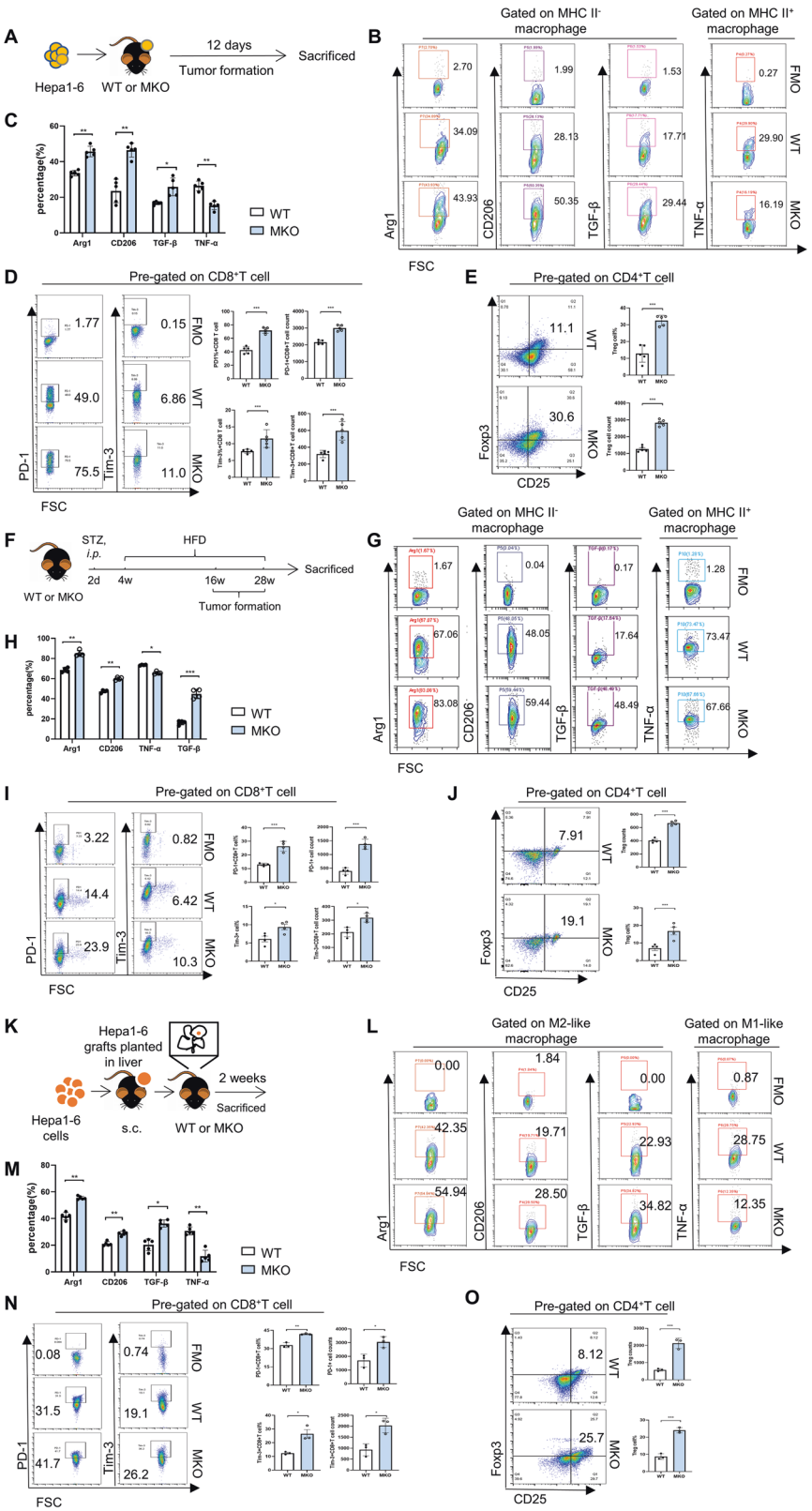

showed the decreased expression of pro-inflammatory genes in the MKO group. By contrast, the anti-inflammatory genes were increased in the MKO group (Fig. 5C). All these data illustrated that Zhx2 is required for macrophages to maintain inflammatory phenotype and function.

To verify the crucial role of Zhx2 in macrophages' inflammatory polarization, BMDMs from MKO and WT mice were stimulated with classical M1 stimuli LPS or M2 stimuli IL-4, and the M1/M2 phenotypes were accessed with an array of genes including immunogenic genes, surface markers and TFs [35]. Compared with

Fig. 4 *Zhx2*-deficient macrophages shared an M2-like phenotype and promoted suppressive T cell infiltration in TME. A–E FACS analysis of TAMs and tumor-infiltrating T cells in liver tumor homograft established by subcutaneously transplanted with Hepa1-6 cells (1×10^6) in WT or MKO mice. **F–J** FACS analysis of TAMs and TILs from STZ-HFD induced liver tumors in WT and MKO mice. **K–O** FACS analysis of TAMs and TILs from WT or MKO mice orthotopically transplanted with Hepa1-6 grafts in the liver. **A**, **F**, and **K** Experimental design, FACs plots (**B, G**, **L**), and bar graphs (**C, H, M**) represent the percentage of Arg1, CD206, TGF-β expression in MHC II$^-$ TAMs and TNF-α expression in M1-like TAMs from WT or MKO mice. **D**, **E**, **I**, **J**, **N**, **O** FCMs analysis of the phenotype of tumor-infiltrated macrophages and T cells from subcutaneous homograft. FACs plots and bar graphs represent percentage and cell counts of Tim-3 and PD-1on CD8$^+$ T cells (**D**, **I**, **N**), and Tregs (**E**, **J**, **O**) in tumor tissues from WT or MKO mice. Treg cell: CD45$^+$Dead$^-$CD3$^+$CD4$^+$CD25$^+$Foxp3$^+$. Fluorescence minus one (FMO) control was used to set gating boundaries. Data are represented as mean ± S.D.Each data point represents an individual mouse. Data were analyzed using Student's *t-test* (two-tailed unpaired t-test) in (**C**–**E**, **H**, **I**, **J**, **M**–**O**), * <0.05, **<0.01, ***<0.001.

WT control, BMDMs from MKO mice displayed significantly repressed expression of M1 markers under LPS stimulation (Fig. 5D–F) but showed enhanced expression of M2 markers after IL-4 treatment (Fig. 5G). Moreover, both the reduced M1 (Fig. 5H, I) and the enhanced M2 phenotypes (Fig. 5J, K) in BMDMs from MKO mice were significantly rescued by Zhx2 overexpression, strongly suggesting the critical role of Zhx2 in controlling macrophages polarization. This was further confirmed in human macrophage cell line THP1 cells (Fig. S9G, H). It was reported that the augmented lactic acid in TME has an important role in the polarization of M2-like TAMs [32], which impelled us to probe the role of Zhx2 in lactate-mediated promotion of M2-like TAMs. As shown in Fig. 5J–M, compared with WT BMDMs, MKO-derived BMDMs showed increased expression of M2-like markers Arg1 and TGF-β under the stimulation of IL-4 (Fig. 5J, K) and lactate (Fig. 5L, M), and this enhanced M2-like polarization of TAMs were largely rescued by *Zhx2* overexpression, which suggested that Zhx2 play roles in TAMs polarization. This was corresponding with our results that lactate reduces Zhx2 expression in TAMs in Fig. 2. Collectively, the above data illustrate Zhx2 as a critical regulator controlling macrophage polarization under different stimuli.

Zhx2 regulates macrophage polarization via transcriptional activation of *Irf1*

To further explore the molecular mechanisms that *Zhx2* deficiency switch macrophages to inflammatory polarization, we further evaluated the DEGs between BMDMs from MKO and WT mice assayed from *PRJNA598552*. GSEA analysis revealed that the top 10 enriched gene sets regulated by Zhx2 mainly focus on pathways related to IRF and NF-κB, the well-defined critical TFs controlling macrophage polarization [36] (Figs. S10A, 6A). Enrichment analysis in TRRUST (https://www.grnpedia.org/trrust/) database also showed that *Irf1* was one of the enriched TFs in DEGs between WT and MKO group (Fig. 6B). To verify whether *Irf1* is the direct target of Zhx2, several molecular biological methods were employed. Realtime-QPCR and immunoblot assays showed that both mRNA and protein levels of Irf1 were greatly reduced in BMDMs under both inflammatory and tumor microenvironmental stimulation or TAMs from MKO mice (Figs. 6C, D, S10B). In accordance, co-transfection and dual luciferase assay demonstrated that *ZHX2* overexpression markedly promoted *IRF1* promoter activity in 293T cells (Fig. 6E). Furthermore, ChIP assay performed with anti-ZHX2 and THP1 cell lysate demonstrated that ZHX2 significantly occupied with *IRF1* promoter (Fig. 6F). The Zhx2 mediated transcriptional activation of *Irf1* was further confirmed with GSEA analysis comparing our RNA-seq data and reported data [37]. As shown in Fig. 6G, Irf1 up-regulated transcripts were greatly enriched in WT subsets compared with the MKO group. All these results suggested that Zhx2 is capable of binding to the *Irf1* locus, thus enhancing *Irf1* transcription.

To validate the involvement of Irf1 in Zhx2-mediated regulation of macrophage polarization and function, *Irf1*-overexpression was performed by lentivirus (*Irf1*-OE) in BMDMs from WT and MKO mice. As shown in Fig. 6H, I, *Irf1* overexpression enhanced the expression of IL-1β, IL-6, and TNF-α in LPS-induced M1-macrophages, and further reversed the reduction of these M1-like proinflammatory cytokines induced by *Zhx2* deficiency. Instead, in IL-4-induced M2-macrophages (Fig. 6J, K) or lactate-induced TAMs (Fig. 6L, M), *Irf1*-overexpression dampened the augmented Arg1, CD206, and TGF-β1 expression in *Zhx2*-knockout BMDMs. To further validate the involvement of Irf1 in Zhx2-mediated regulation of macrophages in tumor inhibition, *Irf1*-overexpression was performed by a lentivirus in BMDMs derived from WT and MKO mice, and these *Irf1*-overexpressing BMDMs were mixed with Hepa1-6 cells and injected subcutaneously to form tumor homografts (Fig. 6N). As shown in Fig. 6O-Q, *Irf1* overexpression significantly dampened the tumor growth in the MKO group. All these data suggest that Zhx2 regulates macrophage polarization by binding to the *Irf1* promoter and thus leading to transcriptional activation of *Irf1*.

NF-κB P65 is required for Zhx2-mediated control of *Irf1* transcription and M1-like polarization of macrophages

To investigate the mechanism of gene-specific targeting of Zhx2 to the *Irf1* gene locus in macrophages, we compared the reported *ZHX2* binding sequence with *IRF1* promoter (−2000 to +1) sequence using JASPAR (http://jaspar.genereg.net/) and PROMO (http://alggen.lsi.upc.es/cgi-bin/promo_v3) database. As shown in Fig. S10C, D, at least three potential ZHX2 binding motifs with overlapping NF-kB-binding sites were found on the *IRF1* promoter (Fig. S10C), among which the motif at −884 to −873 showed the lowest false match rate (Fig. S10D). To evaluate the role of this region in ZHX2-mediated transcriptional regulation of *IRF1*, we generated mutant *IRF1* promoter reporter plasmid which deletes the *GGGAGTCCCA* motif at −884 to −873 (*IRF1*-deletion) and performed co-transfection with *ZHX2* overexpression plasmid (pcZHX2) in 293T cells. Results of dual luciferase assays showed that although ZHX2 markedly enhanced the transcriptional activity of wild-type *IRF1* promoter (*IRF1*-WT) and the deletion of the −884 to −873 motif (*IRF1*-mutant) did not significantly change the *IRF1* promoter activity, ZHX2 lost the ability to regulate the *IRF1*-mutant promoter activity (Fig. 7A), indicating that ZHX2 promotes *IRF1* transcription via *GGGAGTCCCA*.

A previous study has reported that ZHX2 interacts with the p65 protein in renal tumor cells. Accordingly, results of IP with both anti-Zhx2 and anti-p65 showed that Zhx2 interacted with p65 in BMDMs (Fig. 7B). Thus, we proposed that p65 recruits Zhx2 to *Irf1* promoter and regulates *Irf1* transcription in macrophages. In correspondence, ZHX2 and NF-κB p65 shared a series of downstream molecules according to the TRRUST database (Fig. S10E). To further investigate whether the ZHX2-mediated regulation of *IRF1* expression depends on p65 in macrophages, we tested the effect of NF-κB inhibitor (QNZ) (MedChemExpress, *Cat# HY-13812, New Jersey*, U.S.) [38], which could inhibit NF-κB p65 protein phosphorylation and nuclear translocation (Fig. S10F), on ZHX2-mediated *IRF1* expression. While overexpression of *ZHX2* significantly enhanced the activity of *IRF1* reporter, treatment with QNZ efficiently blocked this induction (Fig. 7C). Consistently, while *Zhx2*-deficiency decreased *Irf1* mRNA level, treatment of QNZ markedly eliminated the difference in *Irf1* expression between MKO and WT BMDMs (Fig. 7D). Furthermore, ChIP assay performed with anti-ZHX2 and THP1 cell lysate demonstrated that ZHX2

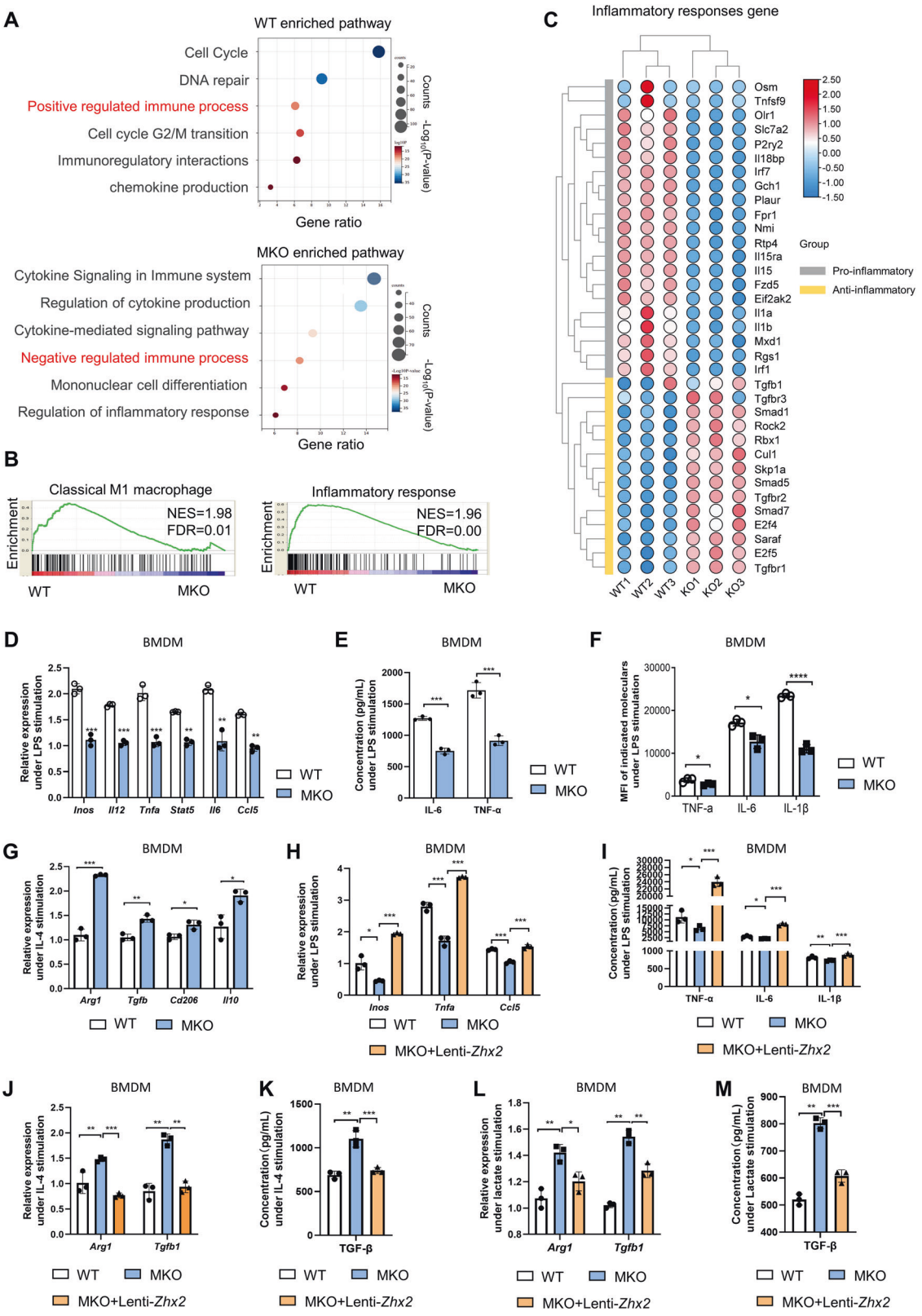

occupied with *IRF1* promoter largely relied on NF-κB p65 phosphorylation and activation since QNZ treatment greatly dampened the accumulation of ZHX2 on *IRF1* promoter in THP1 cells (Fig. 7E). Collectively, above data, strongly suggested that Zhx2 promotes *Irf1* transcription in NF-κB p65 dependent manner.

To validate the involvement of NF-κB p65 in Zhx2-mediated regulation of macrophage polarization and function, QNZ was

Fig. 5 Zhx2 promoted macrophages towards the M1 phenotype. A KEGG pathway analysis of the WT enriched (top) and MKO enriched (bottom) genes in BMDMs. **B** GSEA analysis of the correlation of *Zhx2* expression and classical M1 marker or inflammatory response. **C** Heatmap illustrated the expression of inflammatory response genes in WT and MKO macrophages. BMDMs from WT and MKO mice were stimulated with 100 ng/mL LPS, and the indicated genes were detected in real-timeQPCR (**D**) while protein levels were measured either by ELISA in the cultured medium (**E**) or by FACs in BMDMs (**F**). **G** Realtime QPCR measured the expression of indicated M2-related genes in WT and MKO BMDMs under 20 ng/mL IL-4 stimulation. *Zhx2* overexpression was performed by infection of lentivirus expressing *Zhx2* (lenti-*Zhx2*) in MKO BMDMs and these BMDMs were then stimulated with 100 ng/mL LPS (**H**, **I**), 20 ng/mL IL-4 (**J**, **K**), or 2.5Mm lactate (**L, M**) for 24 h, BMDMs from MKO and WT used as controls. Realtime QPCR analysis of M1-related *Inos, Tnfa, Ccl5* mRNA (**H**) and M2-related *Arg1*, *Tgfb* mRNA (**J**, **L**) is shown, while ELISA measurement of M1-related TNF-α, IL-6, IL-1β level in the supernatant is displayed in (**I**) and M2 related TGF-β level in (**K**, **M**). Data are represented as mean ± S.D. Each data point represents one sample. Data were analyzed using Student's *t* test (two-tailed unpaired t-test) in (**D**–**M**), * <0.05, **<0.01, ***<0.001.

performed in BMDMs from WT and MKO mice. FCM showed that QNZ not only reduced the expression of IL-1β, IL-6, and TNF-α in LPS-induced M1-macrophages but also razed the differences of these proinflammatory cytokines between M1-macrophages from WT and MKO BMDMs (Fig. 7F). ELISA further confirmed the same trends of secretion of IL-1β and IL-6 in BMDMs from WT and MKO (Fig. 7G). These data emphasized a gene-specific activation role of Zhx2-p65 complexes in *Irf1* expression leading to M1 macrophage polarization.

DISCUSSION

Macrophages have a key role in shaping TME, which makes them an important target for cancer treatment [39]. However, modulating macrophages has proved extremely difficult, as we still lack a complete understanding of the molecular and functional diversity of the tumor macrophage compartments. In our study, we identified a checkpoint factor Zhx2 that is vital for programming macrophage polarization, reshaping the immune microenvironment, and inhibiting the progression of liver cancer. Transcription factor Zhx2 is generally characterized as a regulator of several cellular processes including cell differentiation, proliferation, and tumorigenesis. Although Zhx2 is known for its ability to enhance the survival ability and promote the glycolysis of macrophages, the role of Zhx2 in regulating immune-suppressive TAMs is less characterized. Upon focusing on the role of Zhx2 in TAMs, we initially identified Zhx2 as a vital factor that programs macrophage polarization to reshape the immune microenvironment and inhibit the progression of liver cancer. *Zhx2* deficient-TAMs shared a similar phenotype of protumoral-macrophages, which secrete high levels of TGF-β and display anti-inflammatory function, further leading to the immune suppressive microenvironment and increased tumor cell malignancy. By analysis of the profiles of TAMs in HCC patients, we found that the reduced expression of ZHX2 in $CD68^+$ macrophages had a negative correlation with liver cancer patient survival. Constantly, Chen et al. reported that $PFKFB3^+$macrophages infiltration predicts disease progression of human liver cancer [40]. Our results support the biological role of Zhx2 in reprograming TAMs and also suggest a potential therapeutic opportunity.

The tumor microenvironment is typically hypoxic and characterized by a high concentration of lactate, a positive correlation between high lactate levels and tumor progression has been documented in various tumor entities [41, 42]. In our work, we rationalized a conception related to how the complex interplay of tumor microenvironmental signals shape the transcription landscape and thus influences the functional output of TAMs. Compared with the normal medium, the concentration of lactate increased significantly in HCC conditional medium. Consistent with the published data that lactate drives M2 phenotype [43], our data showed that lactate reduced Zhx2 expression in macrophages, and companies by upregulated expression of genes associated with the M2 phenotype. Constantly, results of luciferase assays showed that lactate inhibited the *ZHX2* promoter activity. These findings reveal the importance of lactate in modulating immune cell populations and thereby regulating tumor growth. Zhx2 has been acknowledged as one of the critical locks in macrophages avoiding a transcriptional avalanche [24]. It has been reported that *ZHX2* can be regulated by VHL in tumor cells. Here, in this study, we provided evidence showing that microenvironment stimuli alter ZHX2 expression in macrophages, which might be related to the macrophage's plasticity. Our results that lactate domesticates macrophages through transcriptional regulation of Zhx2, contribute to comprehending the selected polarization of M2-like phenotype of TAMs in the tumor microenvironment. It may be possible to reverse the anti-inflammatory phenotype of TAMs by targeting *ZHX2*, and this may be utilized as a novel approach for macrophage-based immunotherapy. Notably, although lactate is important for *ZHX2* promoter activity, it is not the only factor regulating *ZHX2* transcription, as we also provided data showing that LPS-induced and IL-4 restricted Zhx2 expression.

Our findings identify *Irf1*, as the new downstream target of Zhx2 in regulating the inflammatory responses of macrophages. Irf1 has previously been reported to lead the increased inflammatory cytokine expression in macrophage [44], while impaired IL-4 response [45] and anti-inflammatory M2 macrophage polarization [46]. Our data revealed that ZHX2 occupies a binding site upstream of the transcription start site of *IRF1*, leading to transcriptional activation of *Irf1* and promoting the inflammatory phenotype of macrophages.Irf1 is known as an NF-κB target gene [47] and has been reported to be upregulated by various NF-κB stimuli such as CD40 [48] or TNF-α [49]. We demonstrated that Zhx2 is recruited to the *Irf1* promoter through a protein-protein interaction with NF-κB and thereby regulated *Irf1* expression, which is consistent with the report of *Zhang* et al. showing that ZHX2 binds to p65 protein and regulates NF-κB activation. However, other mechanisms may also exist, as our RNA-seq data showed that *Zhx2*-deficiency reduces *Rela* mRNA expression (data not shown). The detailed mechanism by which Zhx2 regulates NF-κB needs to be further studied.

In conclusion, the data presented in this study suggest that lactate in the liver tumor microenvironment reduces Zhx2 expression in TAMs, which in turn attenuates the immunogenic M1-like activation of macrophage and fosters the liver tumor progression in an NF-κB-Irf1-dependent manner. Our finding highlights the potential role of Zhx2 in the immunogenic phenotype of TAMs in liver cancer and provides a new target aiming at TAMs reprogramming in liver cancer therapy.

METHODS

Animals

Male C57BL/6 mice and mice were pursued from Shandong University Laboratory Animal Center. Myeloid-specific *Zhx2* deficient mice (referred to as "MKO") [26] were generated by crossing $LysM^{cre}$ mice (Jackson Laboratory) and $Zhx2^{f/f}$ mice (gifted by Prof. B. T. Spear, University of Kentucky), sex- and age-matched $LysM^{WT}$, $Zhx2^{f/f}$ mice were used as control (referred as "WT"). All mice were maintained under specific pathogen-free conditions and experiments were carried out under the approval of the Shandong University Laboratory Animal Center.

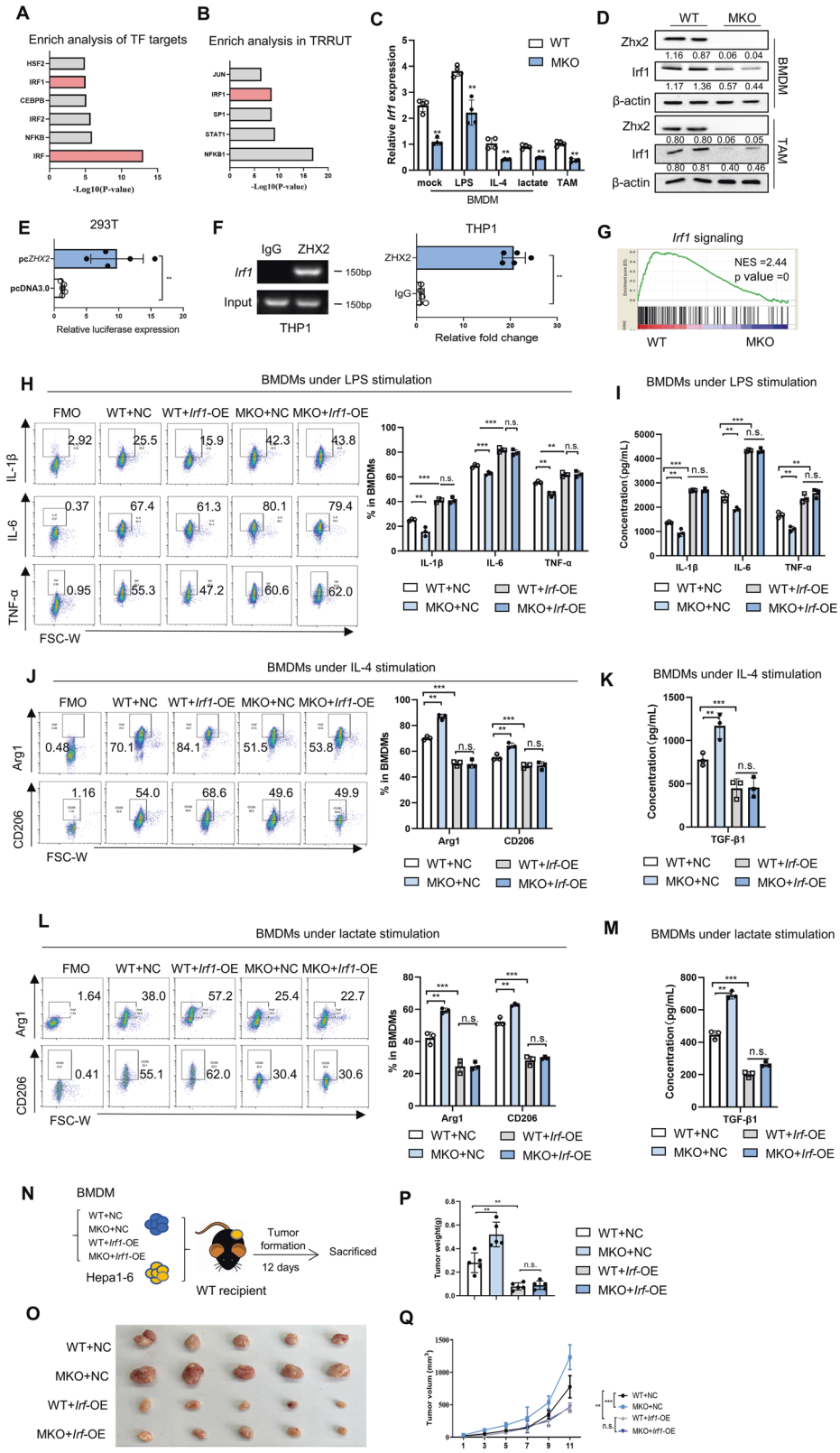

In our study, we used four murine tumor models. (1) Spontaneous NASH-HCC mouse model induced by STZ-HFD as previously described [33]. Briefly, 200ug STZ (Sigma-Aldrich, *Cat#S0130-500MG*, St. Louis, U.S.) was subcutaneously injected into neonatal male mice 2 days after birth. At week 4, mice were fed with HFD (MD12032, Medicines, Jiangsu, China). At week 28, tumor nodes in murine livers were analyzed. (2) Subcutaneous Hepa1-6 homograft model: 1×10^6 Hep1–6 cells were injected subcutaneously into mice. Tumors were measured every other day when reached with a diameter of 3 mm until ~1 cm. The tumor volume was calculated using the formula: volume $= 1/2 \times (\text{length}) \times (\text{width})^2$. To evaluate the pro-tumor function of Zhx2 in macrophage, Hepa1-6 cells, and BMDM were mixed at 1:1 before subcutaneous injection. (3) The orthotopic liver tumor

Fig. 6 Zhx2 directly promotes *Irf1* transcription in macrophages and subsequent inflammatory responses. RNAseq data obtained from WT and MKO BMDMs (*PRJNA598552*) were included and the differentially expressed genes (DEGs) were further analyzed. GSEA functional analysis of enrichment TF targets is shown in (**A**) and analysis of enrichment TF in TRRUT is displayed in (**B**). **C** Realtime QPCR analysis of *Irf1* expression in WT and MKO BMDMs under the indicated treatment or isolated from oncogene-driven liver tumors associated macrophages. **D** Western blotting showed ZHX2 and IRF1 protein levels in BMDMs or TAMs from oncogene-driven liver tumors from WT and MKO mice. β-actin was loaded as a control. **E** Luciferase reporter gene assays were performed in HEK293T cells co-transfected with *ZHX2*-encoding (pc*ZHX2*) or empty (pcDNA3.0) vector and IRF1 promoter reporter plasmid containing −2000 to +100 nt of *IRF1* gene. **F** ChIP assay of ZHX2 binding to *IRF1* promoter in human THP1 cells. PCR Primers were designed across the region around −884 to −873 nt. qPCR analyzed the quantities of foldchange. **G** GSEA analysis of DEGs between BMDMs from WT and MKO and reported *Irf1* signaling (GSE147313). BMDMs from WT or MKO mice were infected with mock lentivirus (NC)/*Irf1* overexpressing lentivirus (*Irf*1-OE). These BMDMs were then stimulated by 100 ng/mL LPS (**H, I**), 20 ng/mL IL-4 (**J**, **K**), or 2.5 mM lactate (**L**, **M**) for 24 h. FCM analysis of IL-1β, IL-6, and TNF-α expression (**H**) or Arg1 and CD206 expression (**J**, **L**). FMO controls were used to set gating boundaries. ELISA measured IL-6, IL-1β, TNF-α (**I**) or TGF-β1 (**K**, **M**) level in supernatant. Tumor growth and weight in MKO mice subcutaneously transplanted with Hepa1-6 cells (1×10^6) mixed with BMDMs (1×10^6) from WT or MKO mice. BMDMs were pretreated with mock lentivirus (NC) or *Irf1* overexpressing lentivirus (*Irf1*-OE). Experimental design (**N**), tumor image (**O**), tumor weight (**P**), and weight (**Q**) are shown. Data are represented as mean ± S.D. Each data point represents one animal. Data were analyzed using Student's *t* test (two-tailed unpaired t-test) in (**C**–**F**, **H**–**M**, **P**) and using two-way ANOVA test in (**Q**), * <0.05, **<0.01, ***<0.001, n.s. no significance.

model: the Hep1-6 tumors were dissected, cut into pieces of ~1 mm^3, and transplanted into the liver parcel of recipient BalB/C mice (male, 6-week-old) as previously reported [23]. (4) The hepatocarcinogenesis driven by *Akt/cMyc*: male (6-week-old) C57BL/6 mice were used for induction of spontaneous liver tumors following hydrodynamic injection of the Sleeping Beauty (SB) transposition system and *Akt/cMyc* plasmid as previously reported [50].

Cell lines

The mouse macrophage cell line RAW264.7, mouse liver tumor cell lines Hepa1-6, and human HCC cell lines Huh7 were obtained from the Cell Resource Center of Shanghai Institutes for Biological Sciences (Shanghai, China). Hepa1-6, Huh-7, and HepG2 were kept at 37 °C at 5%CO_2 in Dulbecco's modified Eagle's Medium (DMEM) supplemented with 10% fetal bovine serum. Raw264.7 were gently scraped when passaged. Human monocyte cell line THP-1 cells were maintained in complete RPMI medium 1640 with 10% FBS and 1% penicillin/streptomycin at 37 °C at 5%CO_2.

Human samples

Surgically resected fresh liver cancer specimens and tissue microarrays were involved in Realtime-QPCR analysis (*Cohort 1*, Table S1) or multiplex IHC staining and overall survival analysis (*Cohort 2* and *3*, Table S2). Tumor tissues and para-tumor tissues were collected from patients with hepatocellular carcinoma. Para-tumor tissues were excised surgically from the area within 2 cm of liver cancer tissues. Two HCC tissue microarrays were got from Qilu Hospital from Shandong University (*Cohort 2*) or purchased from Shanghai SuperFly Biotech (*Cohort 3*) (Shanghai, China). Cohort 2 contained 60 cases of cancerous tissues and 60 cases of paracancerous tissues. Cohort 3 (HLiv-HCC197Sur-01) contained 100 cases of cancerous tissues and 97 cases of paracancerous tissues. This study was approved by the Ethics Committee of Shandong University School of Basic Medical Sciences (Jinan, China), and all patients provided informed written consent.

Multiplexed immunofluorescence staining

Multiplexed immunofluorescence staining of tissue microarray (TMA) was performed using Opal Chemistry (PerkinElmer, Waltham, MA, USA) with antibodies against ZHX2, CD68, and HepPar-1. In Brief, after deparaffinization, TMA slides were processed with microwave (4 min 100% power, 15–20 min 20% power) in antigen retrieval buffer, and blocked with antibody diluent for 10 min at room temperature. Slides were incubated with the primary antibody for 30–60 min, and subsequently incubated with HRP-conjugated secondary antibody for 10 min after removal of the primary antibody and washed in TBST buffer. Thereafter, slides were incubated with Opal working buffer for 10 min at room temperature and then washed in TBST buffer. The above procedures were repeated for other antibodies, and antibodies were removed by microwave treatment (45 s 100% power, 15–20 min 20% power) before another round of staining was performed. Details of antibodies are described in Table S3. Finally, we used DAPI to highlight all nuclei. For Isotype control, TMA was performed using Opal Chemistry with antibodies against CD68, HepPar-1, and IgG (Santa Cruz, Cat# sc-2025), among which IgG was used as a control for ZHX2. The staining conditions for IgG were kept consistent with the anti-ZHX2 antibody.

Multiplexed immunofluorescence image analysis

Visualization and quantitation of the different fluorophores were achieved on the TissueFAXS Spectra Systems and StrataQuest analysis software (TissueGnostics, Vienna, Austria). A multi-spectral image of the whole slide was scanned using a 20× objective lens. Each of the individually stained sections was utilized to establish the spectral library of the fluorophores to eliminate the interference of cross-fluorescence combined with the spectral unmixing algorithm. The contextual tissue cytometry image analysis was applied to analyze the acquired images (StrataQuest, TissueGnostics Vienna, Austria). For phenotype and quantitation analysis, a nuclear segmentation algorithm was applied to the DAPI image to delineate and identify individual cells, and then location information and expression of all the markers were computed for every cell identified. Corresponding algorithms were developed according to different analysis requirements, and then the unified algorithm and the threshold for each channel were applied to all samples of the TMA to standardize the expression and fluorescence level of each marker. The positive areas of cell staining are delineated according to isotype control. The negative fluorescence intensity of CD68 was 2^0–2^6, and the positive staining range of CD68 was 2^6–2^8. The negative fluorescence intensity of ZHX2 was 2^0–2^4, and the positive staining range of ZHX2 was 2^4–2^8. For ZHX2 percentage quantification in TAMs, we first calculated the number of nuclei of $CD68^+$ macrophages in tissues, and further calculated the proportion of ZHX2 positive cell counts of $CD68^+$ macrophage. For ZHX2 mean fluorescence intensity (MFI) quantification, $CD68^+$ macrophages were identified and the MFI of ZHX2 in $CD68^+$ macrophages in each sample was further estimated. For overall survival analysis of HCC patients, tumor regions of HCC tissues were classified into two groups according to $ZHX2^+$ percentage in macrophages. The cut-off for the grouping was determined by the median expression of ZHX2.

Luciferase assay

Pre-cultured cells were transfected with a combination of pGL3-ZHX2, pRL-TK, or pGL3-ZHX2, pRL-TK with ZHX2 overexpressing plasmids (pcZHX2) or mock control (pcDNA3.0). After incubation at 37 °C for 48 h, the transfected cells were collected to analyze firefly luciferase activity using the dual-luciferase reporter assay system (Promega, Wisconsin, USA) according to the manufacturer's protocol and normalized to renilla luciferase activity.

Chromatin immunoprecipitation (ChIP) assays

ChIP assays were performed using a kit (Merck Millipore, MA, USA) according to the manufacturer's protocol. Briefly, THP1 cells were collected, then fixed cells were sonicated to shear DNA to 200–1000 bp and immunoprecipitated using an anti-ZHX2 antibody (Invitrogen, California, USA) or control IgG (Santa Cruz, California, USA). qPCR was performed using specific primers targeting the region of the *Irf1* promoter.

Homogenate preparation

Tumor tissues, and para-tumor tissues used in homogenate preparation were collected from patients with hepatocellular carcinoma. Para-tumor tissues were excised surgically from the area 2 cm away from liver cancer tissues. Tissues were rinsed three times with 10 mL of ice-cold PBS. The washed tissues (2 g) were finely minced and hand-homogenized in 2 mL of PBS using a glass homogenized with a loose-fitting pestle. The resultant

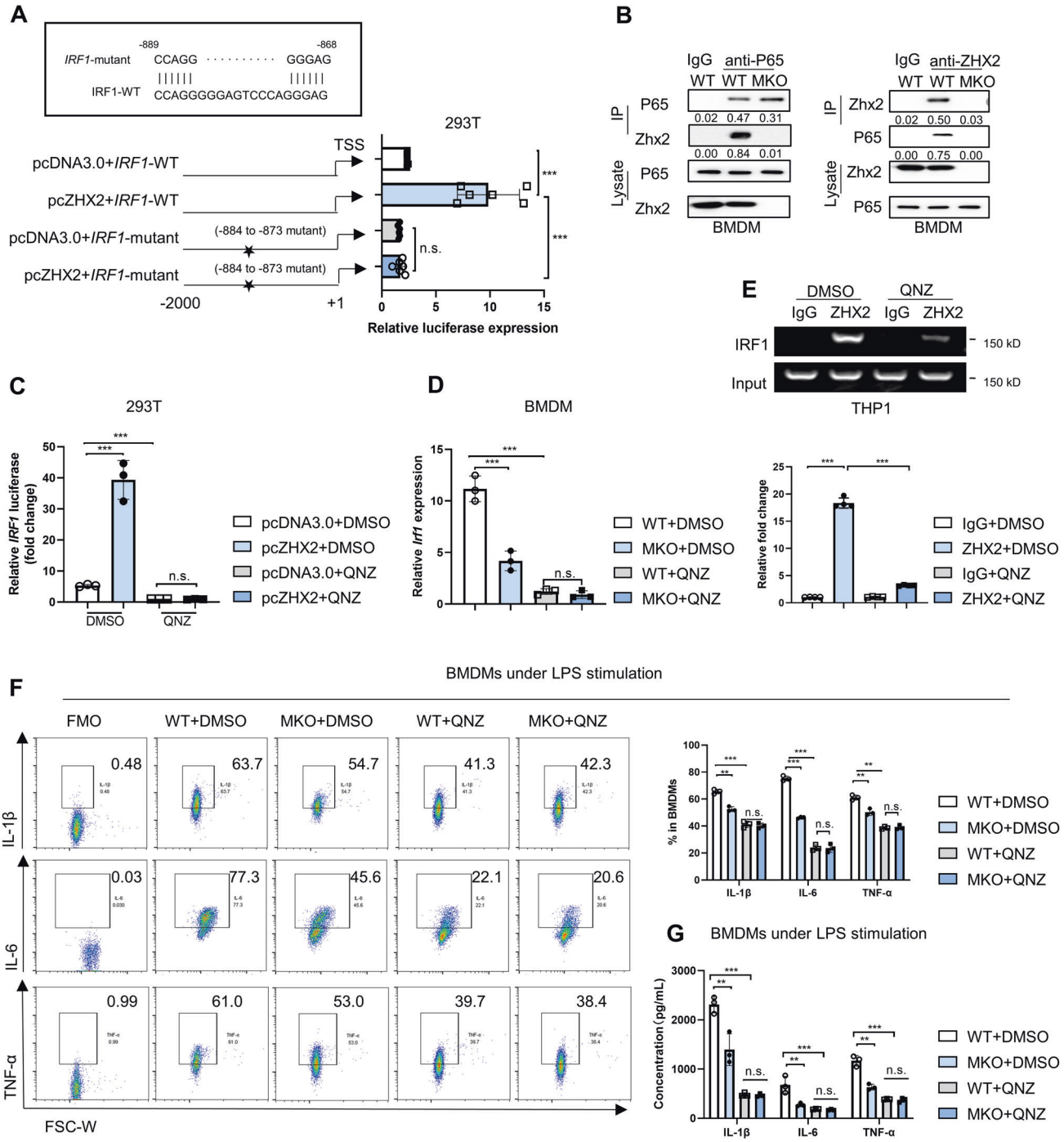

Fig. 7 NF-κB P65 is required for Zhx2 mediated enhancement of *Irf1* transcription and macrophage M1 polarization. A Luciferase assays performed the deleted version of *IRF1* promoter. Positions are shown in base pairs relative to the transcription start site and site-directed-mutate (underlined) are indicated for the constructs. Assays were performed in HEK293T cells cotransfected with *ZHX2* encoding (pc*ZHX2*) or empty vector (pcDNA3.0) for the indicated promoters. **B** The interaction of ZHX2 with NF-κB-P65 in BMDMs was analyzed by Co-IP. **C** Luciferase reporter assays were performed in HEK293T cells co-transfected with *ZHX2*-encoding (pc*ZHX2*) or empty (pcDNA3.0) vector and *IRF1* promoter reporter plasmid containing −2000 ~ + 100 nt of *IRF1* gene. Cells were pre-treated with NF-κB inhibitor (QNZ) or DMSO control. **D** Realtime-QPCR measured *Irf1* mRNA expression in WT and MKO BMDMs with or without QNZ treatment for 12 h. **E** ChIP assay showed ZHX2 binding to *IRF1* promoter in human THP1 cells with or without QNZ treatment. Realtime-QPCR Primers were designed across the region containing −884 to −873 nt. qPCR analyzed the quantities of foldchange. BMDMs from WT or MKO mice pre-treated with QNZ or DMSO control were stimulated by 100 ng/mL LPS for 24 h. **F** FCM analysis of IL-1β, IL-6 and TNF-α expression. FMO controls were used to set gating boundaries. **G** ELISA measured IL-6, IL-1β, and TNF-α level in supernatant. Data are represented as mean ± S.D. Each data point represents one sample. Data were analyzed using Student's *t* test in (**A**, **C**–**G**). (two-tailed unpaired *t* test), * <0.05, **<0.01, ***<0.001, **** <0.0001, n.s. no significance.

homogenate was centrifuged at 200 × *g* for 5 min, and nuclear-free supernatant was designated as the homogenate.

Tissue macrophage isolation

Tumor tissues were cut into small pieces and disrupted with DMEM containing 1 μg/ml collagenase II (Worthington Biochemical, *Cat#LS004177*, Ohio, U.S.) 100 ng/ml hyaluronidase (YEASEN, *Cat#20426ES60, Shanghai, China*) and 0.5 U/ml DNase I (Thermo Fisher Scientific, *Cat#EN0521, Massachusetts, U.S.*) at 37 °C. Tumor-infiltrating lymphocytes (TILs) were separated by human HCC tissues by Ficoil (Tbdscience, *Cat#LTS1077*, Tianjin, China) with 2000 *rpm* and 20 min. The isolated TILs were then cultured in DMEM with 10% FBS for 6 h, allowing collected TAMs to adhere to the culture dish, after being enriched by CD14 magnetic beads (Biolegend, California, USA) (Fig. S1G). For murine TAMs applied to western blotting and RT-QPCR analyses were pre-enriched by F4/80 (Biolegend, California, USA) magnetic beads and further sorted by FACS Aria (Beckman Coulter, Moflo Astrios EQ, California, USA). TAMs were gated and sorted by dead$^-$CD45$^+$CD11b$^+$F4/80$^+$ (Fig. S1B). The purity of the macrophages was >90% for each assay (Figs. S1A, S1B, S1D, S1G).

BMDMs preparation and stimulation

Bone marrow-derived macrophages (BMDMs) were derived by isolating bone marrow from mice aged around 6 weeks old. Bone marrow cells were flushed from femurs and cultured in DMEM with 10%FBS and 100 ng/ml macrophage colony-stimulating factor (PeproTech, *Cat#315-02*, New Jersey, U.S.). Before use in experiments, BMDMs were scraped off from the culture dish, and seeded at 1×10^6 cells per well in 12-well plates. Then BMDMs were stimulated with 100 ng/ml LPS (Sigma, *Cat#L2630*) for M1, 20 ng/ml IL-4 (PeproTech, *Cat#3214-14-50*) for M2, 25 mM lactate (Sigma, *Cat#867-56-1*) and 300 μl supernatants from Hepa1-6 cells cultured in serum-free DMEM for 24 h.

Flow cytometry analysis

Cell suspensions were surface-labeled markers for mouse antibodies for 30 min in the dark at 4 °C. For intracellular staining in macrophages, cells were stimulated with ionomycin (1 μg/ml) (Peprotech, *Cat#5608212-10 mg*) plus PMA (50 nM) (Sigma, Cat#79346) and brefeldin A (Biolegend, *Cat#420601*) for an additional 4 h before harvesting in DMEM with 10% FBS. Then cells were fixed, permeabilized (eBioscience, Cat#*00-5521-00*, California, U.S.), and stained with PBS. The cell count and percentage were detected by CytoFLEX S Flow Cytometer (Beckman Coulter, California, U.S.) or Gallios Flow Cytometer (Beckman Coulter). FCMs were analyzed by Flwojo 10.6 or CytExpert 2.3.0.

Realtime-QPCR

TRIzol reagent (TIANGEN Biotech, *Cat#DP405*, Beijing, China) was applied to harvest total RNA and reverse (R) transcribed into cDNA with RevertAid First Strand cDNA Synthesis Kit (Thermo Fisher Scientific, *Cat#K1622*). The RT-PCR was performed on the ABI Real-Time PCR System with SuperReal PreMix Plus (SYBR Green, TOYOBO, Cat#*QPK-201*, Fukui-ken, Japan). The primers used are shown in Table S4. The conditions used for RT-PCR were as follows: 94 °C for 10 s followed by 40 cycles of 95 °C for 10 s and 60 °C for 20 s. The relative expression of genes was calculated using the $2^{-\Delta\Delta Ct}$ method and β-actin served as an internal control.

Western blot

The proteins from tissues and cells were extracted using cell lysis buffer and rationed by BCA Reagent kit (Beyotime Biotechnology, *Cat#P0012*, Shanghai, China). Equal of protein (50 μg) were loaded in SDS-PAGE, transferred onto polyvinylidene fluoride membranes (Merck Millipore, *Cat#98311*, Darmstadt, Germany), and incubated overnight at 4 °C with the primary Abs from the Table S2. The membranes were washed with PBS with Tween 20 for three times and subsequently incubated with secondary Abs. The signal was detected by enhanced chemiluminescence reagent using the DNR Bio-Imaging Systems (DNR Bio-Imaging Systems, Neve Yamin, Israel).

ELISA

Levels of IL-1β, IL-6, TNF-α, and TGF-β1 were measured by using a commercially available ELISA Kit (Dakewe Biotech, *Cat#1210122, 1210602, 1217202, 102160*, Shenzhen, China) according to the manufacturer's instructions. Briefly, serum or BMDMs cultured medium was added to plates at 37 °C for 90 min, and the unbound materials were removed and washed. After incubation for 30 min with 100 μl streptavidin–HRP, plates were washed and followed with tetramethylbenzidine incubation. Finally, 100-μl/well stop solution was added and read at a wave of 450 nm and a reference wave of 630 nm with an ELISA reader.

RNA-seq analysis

The sequencing data were filtered with SOAPnuke (v1.5.2) by (1) removing reads containing sequencing adapters, (2) removing reads with a low-quality base (base quality ≤ 5) ratio >20%, and (3) removing reads with an unknown base ("N" base) ratio >5%. Afterward, clean reads were obtained and stored in FASTQ format. Raw data were uploaded into the Sequence Read Archive (accession no. PRJNA941106). The clean reads were mapped to the reference genome using HISAT2 (v2.0.4). Bowtiei2 (v.2.2.5) was applied to align the clean reads to the reference coding gene set, and then the expression level of the gene was calculated by RSEM (v1.2.12). Essentially, differential expression analysis was performed using the Poisson algorithm with a false discovery rate (FDR) ≤ 0.001 and |Log2Ratio| ≥1.

To gain insight into the change in phenotype, the Kyoto Encyclopedia of Gene and Genomes (KEGG, https://www.kegg.jp/) enrichment Statistical analysis annotated differently expressed genes was performed by Phyper (https://stat.ethz.ch/R-manual/R-devel/library/stats/html/Hypergeometric.html) based on a hypergeometric test. The significance levels of terms and pathways were corrected by *Q* value with a rigorous threshold ($Q \leq 0.05$) by the Bonferroni correction.

For gene set enrichment analysis (GSEA), we used GSEA (http://software.broadinstitute.org/gsea/index.jsp) software (v3.0) and divided the samples into two groups according to *ZHX2* expression. The molecular signature database (http://www.gsea-msigdb.org/gsea/downloads.jsp) was used to assess pathways and molecular mechanisms. *P* value < 0.05 and FDR < 0.25 were considered statistically significant.

Statistical analysis

Statistical significance was determined using Prism 8.3.0. Two-tail unpaired Student's *t test* between two groups and two-way ANOVA across multiple groups were used to determine significance, and the difference in overall survival was tested using log-rank tests. Data are presented as mean±S.D. Statistical significance was reported as $^*P < 0.05$, $^{**}P < 0.01$, $^{***}P < 0.001$, and *n.s.*, no significance.

Study approval

All mice were maintained under specific pathogen-free conditions and experiments were carried out under the approval of the Shandong University Laboratory Animal Center. Clinical samples were collected from patients after receipt of written informed consent by a protocol approved by The Qilu Hospital of Shandong University.

Reporting summary

Further information on research design is available in the Nature Research Reporting Summary linked to this article.

DATA AVAILABILITY

The RNA sequencing raw data have been deposited in NCBI Sequence Read Archive (SRA) database with the accession number: PRJNA598552. Uncropped original western blots and relevant data are provided in the Supplementary files. The data generated in this study are available upon reasonable request from the corresponding author.

REFERENCES

1. Tang A, Hallouch O, Chernyak V, Kamaya A, Sirlin CB. Epidemiology of hepatocellular carcinoma: target population for surveillance and diagnosis. Abdom Radio. 2018;43:13–25.
2. Jindal A, Thadi A, Shailubhai K. Hepatocellular carcinoma: etiology and current and future drugs. J Clin Exp Hepatol. 2019;9:221–32.
3. Chan S, Wong V, Qin S, Chan H. Infection and cancer: the case of hepatitis B. J Clin Oncol. 2016;34:83–90.
4. Yang Y, Kim S, Seki E. Inflammation and liver cancer: molecular mechanisms and therapeutic targets. Semin Liver Dis. 2019;39:26–42.
5. Ding W, Tan Y, Qian Y, Xue W, Wang Y, Jiang P, et al. Clinicopathologic and prognostic significance of tumor-associated macrophages in patients with hepatocellular carcinoma: a meta-analysis. PloS One. 2019;14:e0223971.

6. Li Z, Wu T, Zheng B, Chen L. Individualized precision treatment: targeting TAM in HCC. Cancer Lett. 2019;458:86–91.
7. Tacke F. Targeting hepatic macrophages to treat liver diseases. J Hepatol. 2017;66:1300–12.
8. Okabe Y, Medzhitov R. Tissue-specific signals control reversible program of localization and functional polarization of macrophages. Cell. 2014;157:832–44.
9. Kawai T, Akira S. The role of pattern-recognition receptors in innate immunity: update on Toll-like receptors. Nat Immunol. 2010;11:373–84.
10. Malyshev I, Malyshev Y. Current concept and update of the macrophage plasticity concept: intracellular mechanisms of reprogramming and M3 macrophage "switch" phenotype. BioMed Res. Int. 2015;2015:341308.
11. Gordon S, Martinez F. Alternative activation of macrophages: mechanism and functions. Immunity. 2010;32:593–604.
12. Vitale I, Manic G, Coussens L, Kroemer G, Galluzzi L. Macrophages and metabolism in the tumor microenvironment. Cell Metab. 2019;30:36–50.
13. DeNardo D, Ruffell B. Macrophages as regulators of tumour immunity and immunotherapy. Nat Rev Immunol. 2019;19:369–82.
14. Heusinkveld M, van der Burg S. Identification and manipulation of tumor associated macrophages in human cancers. J Transl Med. 2011;9:216.
15. Baer C, Squadrito M, Laoui D, Thompson D, Hansen S, Kiialainen A, et al. Suppression of microRNA activity amplifies IFN-γ-induced macrophage activation and promotes anti-tumour immunity. Nat cell Biol. 2016;18:790–802.
16. Cassetta L, Pollard J. Targeting macrophages: therapeutic approaches in cancer. Nat Rev Drug Discov. 2018;17:887–904.
17. Kawata H, Yamada K, Shou Z, Mizutani T, Miyamoto K. The mouse zinc-fingers and homeoboxes (ZHX) family; ZHX2 forms a heterodimer with ZHX3. Gene. 2003;323:133–40.
18. Nagel S, Ehrentraut S, Meyer C, Kaufmann M, Drexler HG, MacLeod RA. Aberrantly expressed OTX homeobox genes deregulate B-cell differentiation in hodgkin lymphoma. PLoS One. 2015;10:e0138416.
19. Zhang J, Wu T, Simon J, Takada M, Saito R, Fan C, et al. VHL substrate transcription factor ZHX2 as an oncogenic driver in clear cell renal cell carcinoma. Science. 2018;361:290–5.
20. Yue X, Zhang Z, Liang X, Gao L, Zhang X, Zhao D, et al. Zinc fingers and homeoboxes 2 inhibits hepatocellular carcinoma cell proliferation and represses expression of Cyclins A and E. Gastroenterology. 2012;142:1559–70.e1552.
21. Lin Q, Wu Z, Yue X, Yu X, Wang Z, Song X, et al. ZHX2 restricts hepatocellular carcinoma by suppressing stem cell-like traits through KDM2A-mediated H3K36 demethylation. EBioMedicine. 2020;53:102676.
22. Wu Z, Ma H, Wang L, Song X, Zhang J, Liu W, et al. Tumor suppressor ZHX2 inhibits NAFLD-HCC progression via blocking LPL-mediated lipid uptake. Cell Death Differ. 2020;27:1693–708.
23. Tan S, Guo X, Li M, Wang T, Wang Z, Li C, et al. Transcription factor Zhx2 restricts NK cell maturation and suppresses their antitumor immunity. J Exp Med. 2021;218:e20210009.
24. Espinal-Enríquez J, González-Terán D, Hernández-Lemus E. The transcriptional network structure of a myeloid cell: a computational approach. Int J Genom. 2017;2017:4858173.
25. Erbilgin A, Seldin MM, Wu X, Mehrabian M, Zhou Z, Qi H, et al. Transcription factor Zhx2 deficiency reduces atherosclerosis and promotes macrophage apoptosis in mice. Arterioscler Thromb Vasc Biol. 2018;38:2016–27.
26. Wang Z, Kong L, Tan S, Zhang Y, Song X, Wang T, et al. Zhx2 accelerates sepsis by promoting macrophage glycolysis via Pfkfb3. J Immunol. 2020;204:2232–41.
27. Mantovani A, Sozzani S, Locati M, Allavena P, Sica A. Macrophage polarization: tumor-associated macrophages as a paradigm for polarized M2 mononuclear phagocytes. Trends Immunol. 2002;23:549–55.
28. Mantovani A, Allavena P, Marchesi F, Garlanda C. Macrophages as tools and targets in cancer therapy. Nat Rev Drug Discov. 2022;21:799–820.
29. Movahedi K, Laoui D, Gysemans C, Baeten M, Stangé G, Van den Bossche J, et al. Different tumor microenvironments contain functionally distinct subsets of macrophages derived from Ly6C(high) monocytes. Cancer Res. 2010;70:5728–39.
30. Christofides A, Strauss L, Yeo A, Cao C, Charest A, Boussiotis V. The complex role of tumor-infiltrating macrophages. Nat Immunol. 2022;23:1148–56.
31. Li Z, Li H, Zhao Z, Zhu W, Feng P, Zhu X, et al. SIRT4 silencing in tumor-associated macrophages promotes HCC development via PPARδ signalling-mediated alternative activation of macrophages. J Exp Clin Cancer Res. 2019;38:469.
32. Colegio OR, Chu NQ, Szabo AL, Chu T, Rhebergen AM, Jairam V, et al. Functional polarization of tumour-associated macrophages by tumour-derived lactic acid. Nature. 2014;513:559–63.
33. Fujii M, Shibazaki Y, Wakamatsu K, Honda Y, Kawauchi Y, Suzuki K, et al. A murine model for non-alcoholic steatohepatitis showing evidence of association between diabetes and hepatocellular carcinoma. Med Mol Morphol. 2013;46:141–52.
34. Yamamoto M, Xin B, Watanabe K, Ooshio T, Fujii K, Chen X, et al. Oncogenic determination of a broad spectrum of phenotypes of hepatocyte-derived mouse liver tumors. Am J Pathol. 2017;187:2711–25.
35. Kang K, Park S, Chen J, Qiao Y, Giannopoulou E, Berg K, et al. Interferon-γ represses M2 gene expression in human macrophages by disassembling enhancers bound by the transcription factor MAF. Immunity. 2017;47:235–50.e234.
36. Mootha V, Lindgren C, Eriksson K, Subramanian A, Sihag S, Lehar J, et al. PGC-1alpha-responsive genes involved in oxidative phosphorylation are coordinately downregulated in human diabetes. Nat Genet. 2003;34:267–73.
37. Cheng Q, Ohta S, Sheu K, Spreafico R, Adelaja A, Taylor B, et al. NF-κB dynamics determine the stimulus specificity of epigenomic reprogramming in macrophages. Science. 2021;372:1349–53.
38. Liao Y, Hua Y, Li Y, Zhang C, Yu W, Guo P, et al. CRSP8 promotes thyroid cancer progression by antagonizing IKKα-induced cell differentiation. Cell Death Differ. 2021;28:1347–63.
39. Ngambenjawong C, Gustafson H, Pun S. Progress in tumor-associated macrophage (TAM)-targeted therapeutics. Adv Drug Deliv Rev. 2017;114:206–21.
40. Chen D, Ning W, Jiang Z, Peng Z, Zhu L, Zhuang S, et al. Glycolytic activation of peritumoral monocytes fosters immune privilege via the PFKFB3-PD-L1 axis in human hepatocellular carcinoma. J Hepatol. 2019;71:333–43.
41. Morrissey S, Zhang F, Ding C, Montoya-Durango D, Hu X, Yang C, et al. Tumor-derived exosomes drive immunosuppressive macrophages in a pre-metastatic niche through glycolytic dominant metabolic reprogramming. Cell Metab. 2021; 33:2040–58.e2010.
42. Wei G, Sun H, Dong K, Hu L, Wang Q, Zhuang Q, et al. The thermogenic activity of adjacent adipocytes fuels the progression of ccRCC and compromises anti-tumor therapeutic efficacy. Cell Metab. 2021;33:2021–39.e2028.
43. Zhang J, Muri J, Fitzgerald G, Gorski T, Gianni-Barrera R, Masschelein E, et al. Endothelial lactate controls muscle regeneration from ischemia by inducing M2-like macrophage polarization. Cell Metab. 2020;31:1136–53.e1137.
44. van der Vorst E, Theodorou K, Wu Y, Hoeksema M, Goossens P, Bursill C, et al. High-density lipoproteins exert pro-inflammatory effects on macrophages via passive cholesterol depletion and PKC-NF-κB/STAT1-IRF1 signaling. Cell Metab. 2017;25:197–207.
45. Piccolo V, Curina A, Genua M, Ghisletti S, Simonatto M, Sabò A, et al. Opposing macrophage polarization programs show extensive epigenomic and transcriptional cross-talk. Nat Immunol. 2017;18:530–40.
46. Huang R, Hu Z, Chen X, Cao Y, Li H, Zhang H, et al. The transcription factor SUB1 is a master regulator of the macrophage TLR response in atherosclerosis. Adv Sci. 2021;8:e2004162.
47. Eckhardt I, Weigert A, Fulda S. Identification of IRF1 as critical dual regulator of Smac mimetic-induced apoptosis and inflammatory cytokine response. Cell Death Dis. 2014;5:e1562.
48. Moschonas A, Kouraki M, Knox P, Thymiakou E, Kardassis D, Eliopoulos A. CD40 induces antigen transporter and immunoproteasome gene expression in carcinomas via the coordinated action of NF-kappaB and of NF-kappaB-mediated de novo synthesis of IRF-1. Mol Cell Biol. 2008;28:6208–22.
49. Andersen P, Pedersen M, Woetmann A, Villingshøj M, Stockhausen M, Odum N, et al. EGFR induces expression of IRF-1 via STAT1 and STAT3 activation leading to growth arrest of human cancer cells. Int J Cancer. 2008;122:342–9.
50. Wang C, Cigliano A, Jiang L, Li X, Fan B, Pilo M, et al. 4EBP1/eIF4E and p70S6K/RPS6 axes play critical and distinct roles in hepatocarcinogenesis driven by AKT and N-Ras proto-oncogenes in mice. Hepatology. 2015;61:200–13.

ACKNOWLEDGEMENTS

This study was supported in part by the National Key Research and Development Program (2021YFC2300603), the National Science Foundation of China (Key program 81830017, 8223056, 32200742), Taishan Scholarship (No.tspd20181201), Major Basic Research Project of Shandong Natural Science Foundation (No. ZR2020ZD12), the Shandong Provincial Natural Science Foundation (ZR2021QH322, ZR2019PH023) and Collaborative Innovation Centre of Technology and Equipment for Biological Diagnosis and Therapy in Universities of Shandong. We also thank the Translational Medicine Core Facility of Shandong University for the consultation and instrument availability that supported this work.

AUTHOR CONTRIBUTIONS

CM, ST, and ZW formulated the study concept and designed the studies. ST, ZW, NL, XG, YZ, HM, XP, and YZ performed the experiments. ST, ZW, and CM analyzed the results. CL, LG, TL, XL, and CM interpreted the results. ST, ZW, and CM wrote and edited the manuscript.

COMPETING INTERESTS

The authors declare no competing interests.

ADDITIONAL INFORMATION

Supplementary information The online version contains supplementary material available at https://doi.org/10.1038/s41418-023-01202-4.

Correspondence and requests for materials should be addressed to Xiaohong Liang or Chunhong Ma.

Reprints and permission information is available at http://www.nature.com/reprints

Publisher's note Springer Nature remains neutral with regard to jurisdictional claims in published maps and institutional affiliations.